RSC Advances

PAPER

View Article Online
View Journal | View Issue

Cite this: *RSC Adv.*, 2024, **14**, 18148

Removal mechanism of Pb(II) from soil by biochar-supported nanoscale zero-valent iron composite materials

Shuxian Wei,[a] Gang Du,[a] Canhua Li, *[ac] Lanyue Zhang,[a] Jiamao Li,*[b] Aiqin Mao[b] and Chuan He[d]

As an adsorbent, biochar has a highly porous structure and strong adsorption capacity, and can effectively purify the environment. In response to the increasingly serious problem of heavy metal pollution in water, this study used nano zero valent iron and rice husk biochar to prepare a new type of magnetic sheet-like biochar loaded nano zero valent iron (BC-nZVI) composite material through rheological phase reaction, showing remarkable advantages such as low cost, easy preparation, and superior environmental remediation effect. The physical and chemical properties and structure of the material were extensively characterized using various methods such as HRTEM, XPS, FESEM, EDS, XRD, FTIR, and RAMAN. Concurrently, batch experiments were undertaken to assess the removal efficiency of Pb(II) by BC-nZVI, with investigations into the influence of pH value, temperature, soil water ratio, and initial concentration of heavy metal ion solution on its removal efficiency. The results indicate that the removal of Pb(II) by BC-nZVI reaches an equilibrium state after around 120 minutes. Under the conditions of pH 6, temperature 20 °C, soil water ratio 1 : 5, and BC-nZVI dosage of 1 g L^{-1}, BC-nZVI can reduce the Pb(II) content in wastewater with an initial concentration of 30 mg L^{-1} to trace levels, and the treatment time is about 120 minutes. The analysis of adsorption kinetics and isotherms indicates that the adsorption process of Pb(II) by BC-nZVI adheres to the quasi-second-order kinetic model and Langmuir model, suggesting a chemical adsorption process. Thermodynamic findings reveal that the adsorption of Pb(II) by BC-nZVI is spontaneous. Furthermore, BC-nZVI primarily accumulates Pb(II) through adsorption co-precipitation. BC-nZVI serves as an eco-friendly, cost-effective, and highly efficient adsorbent, showing promising capabilities in mitigating Pb(II) heavy metal pollution. Its recoverability and reusability facilitated by an external magnetic field make it advantageous for remediating and treating lead-contaminated sites.

Received 7th May 2024
Accepted 31st May 2024

DOI: 10.1039/d4ra03357d

rsc.li/rsc-advances

1 Introduction

As the chemical industry advances swiftly, wastewater laden with lead from specific industrial sectors like battery manufacturing facilities, metal smelting plants, sewage treatment plants, and printing and dyeing factories, can readily infiltrate groundwater. Research has shown that the soil of lead and zinc smelting sites in China has a high content of lead and zinc, with the highest concentration of lead reaching over 310 000 mg kg^{-1}. Lead is a typical heavy metal, and its pollution in the soil has characteristics such as concealment, aggregation, and irreversibility, making it difficult to degrade through natural systems.[1,2] As a result, the search for cost-effective methods to manage lead pollution and restore normal crop growth and human health has become a key focus in environmental science research.[3]

In recent years, the application of engineered magnetic nanoparticles has become common in the areas of wastewater treatment and remediation.[4] Nano zero valent iron (nZVI) can be produced by several methods. Earlier techniques included

[a]*School of Metallurgical Engineering, Anhui University of Technology, Ma'anshan, Anhui 243002, China. E-mail: wsx1983246954@163.com; licanhua1979@163.com; Tel: +8618162347179*

[b]*School of Materials Science and Engineering, Anhui University of Technology, Ma'anshan, Anhui 243002, China*

[c]*Anhui Province Key Laboratory of Metallurgical Engineering & Resources Recycling, Ma'anshan, Anhui 243002, China*

[d]*Jiuquan Vocational and Technical College, Jiuquan, GanSu, 735000, China*

Shuxian Wei (1999), male, master's student, mainly focuses on the green preparation of ecological materials.

Li Canhua (1979), male, PhD, professor, mainly focuses on ecological security and environmental hazard control, and the preparation of nanomaterials.

physical processes like grinding, abrasion, and lithography. Nowadays, a more favored approach is the preparation through nucleation, phase separation, or high-temperature annealing of uniform solutions or gases. In addition to the above methods, there are many chemical methods available for synthesizing nZVI, such as using sodium borohydride ($NaBH_4$) as a reducing agent, carbon thermal reduction, electrochemical method, green synthesis, ultrasound assisted synthesis, *etc*[5]. However, these methods have drawbacks such as high raw material costs, toxic and explosive by-products, hazardous processes, and high energy consumption. The main objectives of the development of new methods for the production of nZVI and the modification of nZVI are to reduce the cost of production and to improve its stability, which will lead to a wider use of nZVI in practice.

Biochar (BC) is a porous carbon material created through the pyrolysis of biomass in either anaerobic or oxic environments. The raw materials for preparing BC are diverse, such as municipal sludge, waste eggshells, animal manure, and agricultural waste.[6] Due to its large specific surface area and rich microporous structure and active functional groups, biochar has become an effective and cost-effective soil remediation material.[7] At present, the use of nZVI and carbon based nanocomposites for environmental remediation of water, soil, and other environments has become one of the hot topics of widespread concern for many scholars at home and abroad. Peng[8] *et al.* found that the fixation rate of Pb in polluted soil by nZVI/biochar (54.6%, 90 day reaction) was much higher than that of Fe_3O_4/biochar (30.5%). Lu[9] *et al.* adopted green sustainability derived from biosynthesis carbon@nano Zero valent iron composite material (C@nZVI) can remove 98.7% of lead from actual mining wastewater. Qian[10] *et al.* studied the use of nanoparticle zero valent iron loaded on porous biochar for immobilizing cadmium (Cd) and lead (Pb) in cohesive soil. The BC-nZVI process was superior to the BC or nZVI process in immobilizing Cd or Pb, with approximately 80% heavy metal immobilization obtained. These studies have shown that biochar/nZVI is a promising technology for remediating various heavy metals in soil, with demonstrated effectiveness in real-world applications.

This study aims to investigate an affordable and straightforward approach for extracting lead ions from soil, employing rice husk biochar infused with zero-valent iron (BC-nZVI). Magnetizable sheet-shaped BC-nZVI materials were prepared by utilizing $FeCl_2 \cdot 4H_2O$ and rice husk biochar through a rheological phase reaction. The physical and chemical properties, as well as the fine structure of the materials, were characterized in detail using various techniques such as Field-Emission Scanning Electron Microscope(FESEM), Energy-Dispersive X-ray Spectroscopy(EDS), High-Resolution Transmission Electron Microscopy (HRTEM), X-ray Diffraction (XRD), X-ray Photoelectron Spectroscopy (XPS), Raman Spectroscopy (RAMAN), Fourier Transform Infrared Spectroscopy (FTIR). In the study, the effects of lead ion concentration, soil–water volume ratio, pH value, and temperature on the lead removal efficiency were investigated. The results demonstrated that the combination of rice husk biochar and nano zero-valent iron effectively removed lead ions from the soil. At the same time, we thoroughly investigated the adsorption characteristics of the composites on Pb^{2+} and explored the adsorption mechanism of nZVI in the treatment of heavy metals, aiming to find an economical and efficient method to treat Pb^{2+}-containing wastewater. This study holds importance not only in addressing lead pollution and engineering challenges linked to agricultural waste reuse but also in its broader implications for managing lead contamination and agricultural waste resource utilization. The findings present a viable and cost-effective approach to treating lead-contaminated wastewater.

2 Experimental

2.1 Materials and reagents

Tetrahydrate ferrous chloride ($FeCl_2 \cdot 4H_2O$), sodium thiosulfate ($Na_2S_2O_2$), lead chloride ($PbCl_2$), lead national standard sample (Pb), sodium hydroxide (NaOH), hydrochloric acid (HCl), sodium chloride (NaCl), and high-purity nitrogen gas (99% purity). These chemicals are all of analytical grade and were purchased from Shanghai Maclyn Biochemical Technology Co., Ltd. The rice husk biochar was obtained from Ma'anshan City, Anhui Province, China. They were prepared into the required solutions using deionized water.

2.2 Instrumentals

Scanning and transmission electron microscope (SEM, JSM-6490LV, Japan; TEM, FEI-TALOS-F200X, Japan) and brunner emmet teller (BET, ASAP 2460, USA) were used to observe surface morphologies and pore size distributions of BC, and BC-nZVI. The characteristic groups of BC, and BC-nZVI were detected by fourier spectra (FT-IR, Nicolet iS20, America). X-ray diffractometer (XRD, Ultima IV, Japan) was used to explore the crystallographic structures of BC, and BC-nZVI. Carbonization degrees of BC, and BC-nZVI after washing were revealed by Raman spectra (Raman, inVia, Britain). X-ray photoelectron spectroscopy (XPS, Thermo Kalpha, America) was used for observing chemical elements (C and Fe) changes of BC-nZVI before and after reaction.

2.3 Adsorption tests

2.3.1 Preparation of biochar-supported nanoscale zero-valent iron. Strict anaerobic procedures must be followed during all processes involving $FeCl_2 \cdot 4H_2O$ to prevent oxidation of Fe(II) to Fe(III). 20 g of granular NaOH, 20 g of $Na_2S_2O_2$, and 5 g of rice husk biochar that had been screened through a 100-mesh sieve were weighed out. During stirring, contact with moisture should be avoided, and humidity and temperature should be controlled in a glove box to prevent NaOH from absorbing water. The three solid materials were thoroughly mixed to obtain a solid mixture. The mixture was transferred to a beaker and sealed for storage in a glove box rich in nitrogen gas.

The preparation of BC-nZVI composite material was carried out in a glove box under N_2 protection. The mixed reactants were placed in an ice bath and mixed using a spray bottle while spraying water until the reactants reached a rheological phase and the reaction began. After continuous stirring for a specified

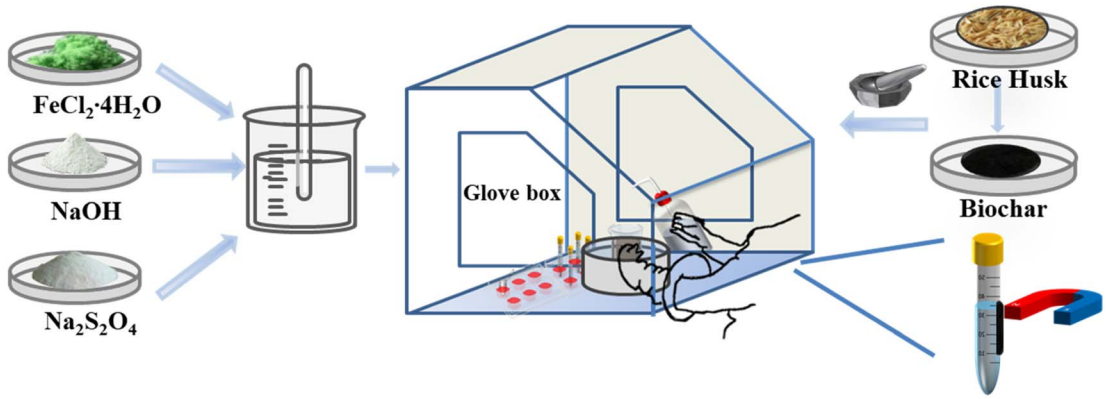

Fig. 1 Schematic diagram of the preparation of BC-nZVI.

duration, the reaction mixture was allowed to cool to room temperature. Once the reaction concluded, the cooled product underwent filtration under nitrogen shielding. Subsequently, it was repeatedly washed with oxygen-free distilled water and anhydrous ethanol to isolate the prepared BC-nZVI particle solution. The particle solution was then subjected to ultrasonic cleaning, with centrifugal sedimentation and removal of the supernatant, until the pH reached neutral. Finally, the BC-nZVI composite material was obtained through vacuum drying. The detailed process flow diagram of the synthesis related to BC-nZVI is shown in Fig. 1.

2.3.2 Experimental methods for heavy metal removal. Initially, a stock solution containing the necessary ions was prepared using heavy metal salts. A stock solution of Pb(II) was created by dissolving $PbCl_2$ to reach a concentration of 1 mg mL^{-1}. Following this, the stock solution was gradually diluted with deionized water according to the experimental parameters. 100 mL of the diluted stock solution was then transferred to a 250 mL conical flask and placed in a thermostatic oscillator set at 20 °C and a rotational speed of 200 rpm. A certain amount of BC-nZVI was added to the system. The samples were collected at regular intervals, filtered through a 0.22 μm membrane, and analyzed using atomic absorption spectrophotometry. Two parallel experiments were conducted to correct for possible errors. The calculations for the removal amount (Q_t) and removal efficiency (η) of Pb(II) by the material are as follows:

$$Q_t = (C_0 - C_t) \times V/m \quad (1)$$

$$\eta = (C_0 - C_t)/C_0 \times 100\% \quad (2)$$

In the equation, C_0 represents the initial concentration (mg mL^{-1}) of Pb(II) at time $t = 0$, C_t represents the concentration (mg mL^{-1}) of Pb(II) at time t, V represents the volume (L) of the solution, and m represents the amount (mg) of the material added.

3 Results and discussion

3.1 Characterization of BC-nZVI

3.1.1 FESEM and HRTEM characterization analysis. The morphology of the BC-nZVI composite was analyzed using field emission scanning electron microscopy (FESEM). As illustrated in Fig. 2(a), nZVI particles exhibit uniform dispersion across the BC surface, forming a coherent sheet-like structure.This indicates that loading BC effectively reduces the degree of nZVI aggregation. Fig. 2(g) shows that nZVI particles are fixed onto the surface of BC while the degree of aggregation is significantly reduced. Further magnification observation reveals that these particles form a clear sheet-like structure with a diameter between 50–1500 nm and a thickness less than 50 nm. The energy-dispersive X-ray spectroscopy (EDS) results of the boxed region in Fig. 2, as shown in Fig. 2(b–f), reveal that the main elements of the nanosheets are Fe, C, Si, and O. Among these, Si content stands out for its relative richness, primarily stemming from the typical abundance of silica carbon in rice husk biochar.[11]

Further observation through HRTEM reveals the TEM image of some nanosheets in Fig. 2(h). At higher resolution in Fig. 2(h) and (i), a dark and mottled structure can be observed within individual nanosheets. Several concentric rings in the SAED pattern correspond to the diffraction of C's (200) and (210) crystal planes, SiO_2's (112) crystal plane, and α-Fe's (110) and (200) crystal planes.[12] Fig. 2(i) and (l) depict the crystal structures of the dark and light regions, where the lattice spacing of the dark region is measured to be 2.0267 Å, corresponding to the body-centered cubic (110) planes of α-Fe, while the outer light region corresponds to the (211) crystal plane of C. It can be confirmed that α-Fe is successfully loaded onto the surface of the biochar carrier in nanosheet form, with a distance exceeding 100 nm from the edges, confirming the successful loading of nZVI. Fig. 2(l) clearly shows the presence of dark areas representing the sheet-like nano zero-valent iron loaded on the surface of the biochar. Additionally, the line-scanning TEM images in Fig. 2(j) and (k) reveal that the primary elements present in the nanosheets are C, Fe, and O.[13] Subsequent experiments have observed an ideal heavy metal adsorption capacity, indicating that biochar material is an effective carrier that can address issues related to nZVI aggregation and oxidation, which may otherwise lead to a decrease in activity of nZVI. Based on XRD analysis, it has been found that the biochar matrix contains a relatively high content of Fe^0. This

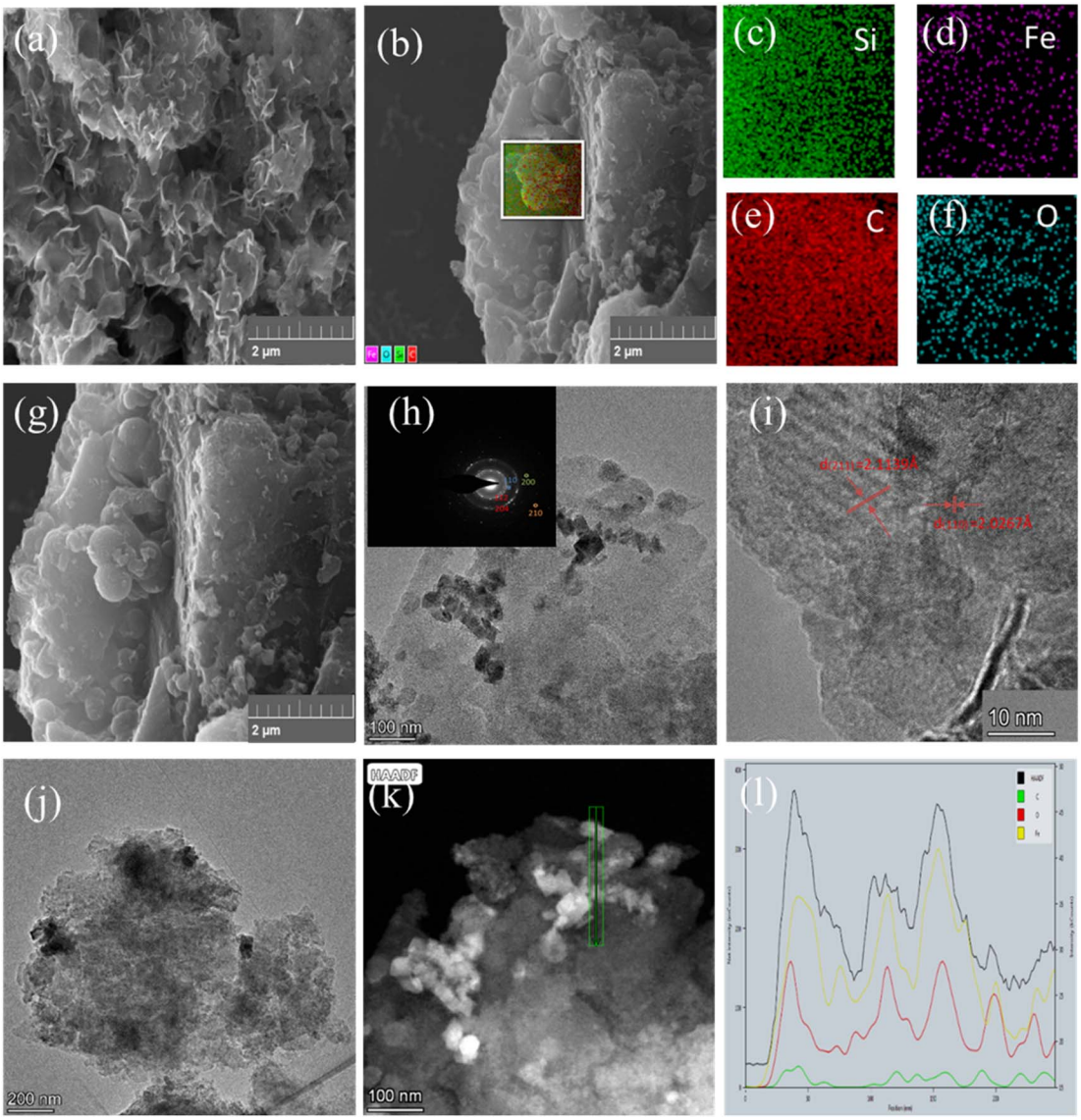

Fig. 2 SEM images (a, b, g), EDS energy spectrum scanning (c–f), TEM images (h–j), and line scanning (k–l) of BC-nZVI.

suggests that most of the Fe^0 is located within the pore structure of the biochar or encapsulated by it, resulting in a lower content of surface zero-valent iron. Previous studies have also reported on the typical core–shell structure of Fe^0, which means that it is coated by iron oxides to effectively prevent oxidation.

3.1.2 XRD and FTIR characterization analysis. Fig. 3(a) and (b) display the X-ray diffraction (XRD) pattern and Fourier transform infrared (FTIR) spectrum of BC-nZVI. In Fig. 3(a), the peaks at 44.67°, 65.02°, and 82.33° in 2θ correspond to the α-Fe crystal structure. Additionally, the diffraction peaks of SiO_2 are observed at 21.7°, 26.6°, 39.0°, and 47.2° in 2θ. This suggests that the main reaction products are α-Fe and SiO_2, with some SiO_2 potentially originating from partially burned rice husks. However, no diffraction peak corresponding to C is detected in the XRD spectrum, possibly due to the generation of a significant amount of amorphous carbon during chemical reactions. Therefore, further analysis using Raman spectroscopy was conducted, as shown in Fig. 3(f). The two prominent peaks in the figure are located at approximately 1360 and 1580 cm^{-1}, representing the characteristic signals of disordered carbon (D-band) and graphite carbon (G-band), respectively.[14] The D-band signifies the presence of a disordered aromatic ring structure in carbon materials,[15–17] while the G-band corresponds to the vibration and stretching of sp^2 orbitals in carbon rings or chains. Some researchers attribute the G-band to the presence of a graphite carbon structure in the material.[18]

In Fig. 3(b), the FTIR spectrum of BC-nZVI is displayed. The absorption peaks noted at approximately 3400 and 1630 cm^{-1} are attributed to the stretching vibration of surface hydroxyl groups (–OH) and the bending vibration of water molecules (H–O–H), respectively.[19]

According to literature,[20] metal oxides are typically covered with hydroxyl groups, which can exist in different forms at different pH values, leading to the variations in surface charge

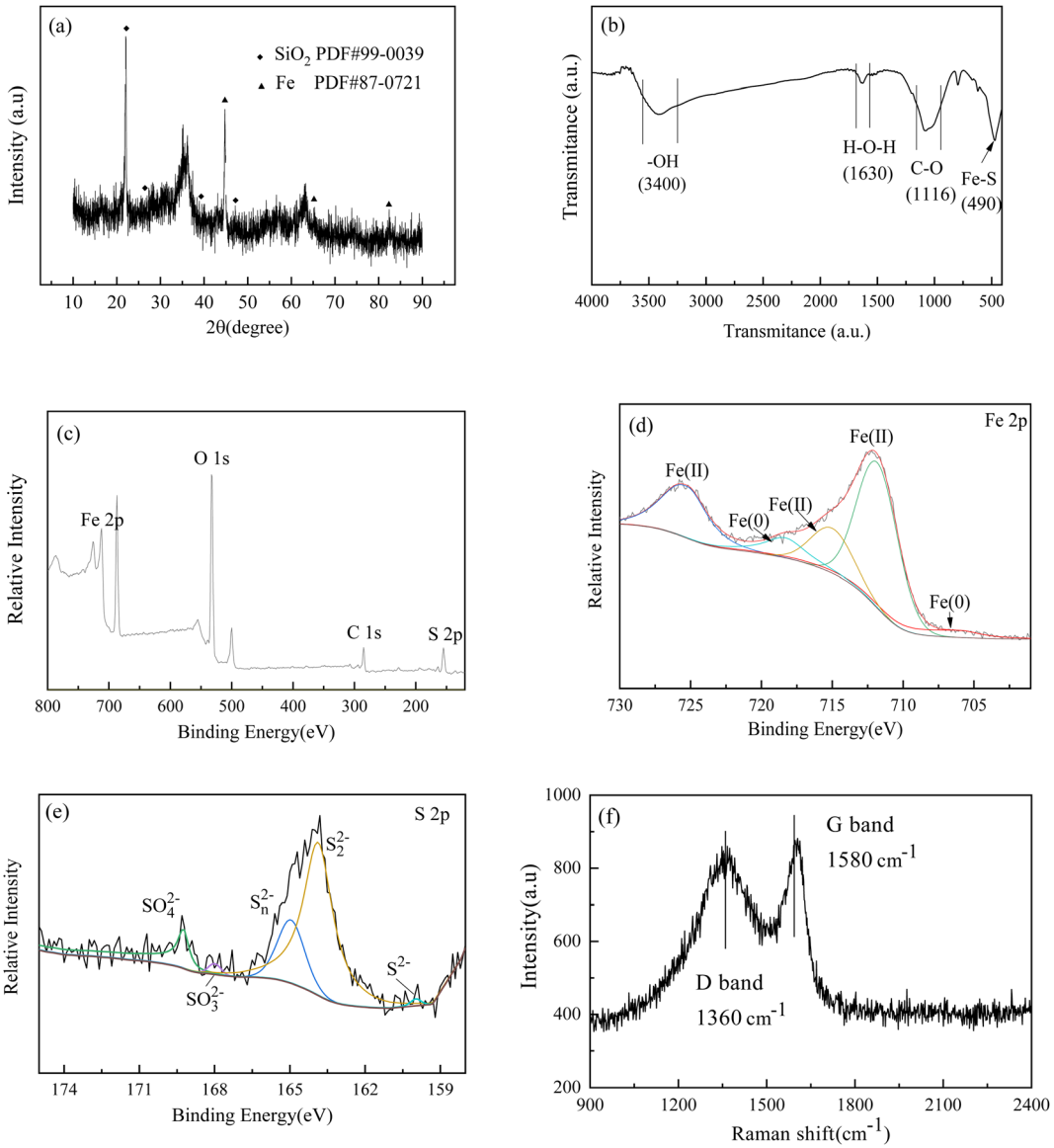

Fig. 3 XRD pattern (a). FTIR spectrum (b), XPS full spectrum (c), Fe 2p, S 2p fine spectrum (d–f) and Raman spectrum (e) of BC-nZVI.

of BC-nZVI with various pH values. The peak observed at 1116 cm^{-1} is associated with the stretching vibration of C–O, signifying the existence of surface functional groups on the biochar with elevated oxygen content, such as hydroxyl (–OH) or carboxyl (H–*O*–H) groups. These functional groups can form coordination bonds with iron ions and be adsorbed onto the surface of BC-nZVI. The peak on the right-hand side of 500 cm^{-1} is related to the stretching vibration of Fe–S in BC-nZVI. During the preparation of biochar-supported nano zero-valent iron materials, these functional groups can adsorb Fe(II) from the solution, facilitating the loading of nano zero-valent iron.

3.1.3 XPS characterization analysis. XPS analysis provides comprehensive chemical characterization details regarding the synthesized samples. Fig. 3(c) presents the XPS spectrum of BC-nZVI, wherein the binding energy peaks of S 2p, O 1s, C 1s, and Fe 2p are arranged in ascending order of energy levels.

In the Fig. 3(d), the characteristic peaks of 708.9 eV and 719.7 eV are considered Fe^0, 710.1 eV and 724.5 eV representing Fe^{2+}, indicating that Fe is the main iron species in the nanomaterials. Outside the core–shell structure, the valence states of iron are mainly Fe(II) and Fe(III). Fig. 3(e) indicates that the formation of the dominant layer on the surface of BC-nZVI can increase the reactivity of nanomaterials. Five characteristic peaks were obtained by fitting the S 2p spectrum, with peaks located at 169.2, 167.8, 163.9, 162.9, and 160.9 eV corresponding to six sulfur compounds (SO_42-, SO_32-, SO_n2-, S_22- and S2−). In addition, some S is oxidized to form oxides during the synthesis process.[21,22] In summary, the surface shell of BC-nZVI composite nanomaterials primarily comprises sulfur oxides with a minor presence of iron (hydrogen) oxides.

In Fig. 3(d), Fe 2p peaks exhibiting spin–orbit splitting are evident at positions 706.8 and 723.5 eV. These signals originate from photoelectrons emitted by Fe (0), Fe(II), and Fe(III),

respectively. A slight enhancement in the Fe(0) signal is noticeable, albeit weak, suggesting that α-Fe is not uniformly dispersed and precipitated within the Fe_3O_4 matrix. Consequently, BC-nZVI likely possesses a core–shell structure, with Fe(0) situated at the core position.[23] This is similar to the research results of other scholars,[24,25] where the oxide shell of nano zero valent iron mainly contains FeOOH, FeO, α/γ- Fe_2O_3 and Fe_3O_4.[26]

3.2 The effect of initial Pb^{2+} concentration on its adsorption efficiency

Under the conditions of pH of 6, temperature of 20 °C, soil–water volume ratio of 1 : 5, and BC-nZVI dosage of 1 g L^{-1}, the impact of various initial concentrations of Pb(II) on its removal rate was examined. As shown in Fig. 4, BC-nZVI demonstrates effective removal of Pb(II) from wastewater, particularly at lower initial Pb(II) concentrations. In particular, when treating the wastewater with an initial concentration of 30 mg L^{-1}, the Pb(II) content could be reduced to a trace level in only about 120 minutes, and the removal rate reached 100%, indicating that BC-nZVI had more active sites available for heavy metals to occupy. However, as the initial concentration of Pb(II) increases, the removal rate gradually decreases. At an initial Pb(II) concentration of 50 mg L^{-1}, the final removal rate decreases to 65.74%, possibly attributed to the limited availability of binding sites on the BC-nZVI surface, leading to reduced Pb(II) removal efficiency. Therefore, when treating high-concentration wastewater, it is necessary to increase the dosage of BC-nZVI or adopt other treatment methods to improve the removal efficiency. BC-nZVI can efficiently remove Pb(II) from aqueous solutions, and the three control groups with different initial concentrations reach equilibrium at around 120 minutes, indicating that BC-nZVI has a strong removal effect on Pb(II). It shows extremely high effluent quality when removing low-concentration wastewater, which overcomes the problem that low-concentration Pb(II) is difficult to remove from water using traditional lime precipitation.[27]

3.3 The effect of different soil-to-water ratios on the adsorption efficiency of Pb^{2+}

In the reaction of BC-nZVI material with Pb(II) in soil, the experiment has two main processes, firstly, the extraction of Pb^{2+} by water, which depends on the soil–water volume ratios, and secondly, the exploration of the adsorption of Pb^{2+} on the surface of the composite material. The soil–water ratio will have an effect on the oxidation rate of zero-valent iron nanoparticles and the leaching effect of Pb(II) from the soil. The initial concentration of Pb(II) was set at 30 mg L^{-1}, with a pH value of 6 and a temperature of 20 °C. The dosage of BC-nZVI was 1 g L^{-1}. The results are shown in Fig. 5(a).In the absence of zero-valent iron material, as the soil–water volume ratio of 1 : 5 increases, one group of samples shows a gradual increase in the removal amount and removal efficiency of Pb(II), but the rate of increase is relatively slow. When the soil-to-water volume ratio increases from 1 : 10 to 4 : 10, the removal amount and removal efficiency of Pb(II) in the soil by BC-nZVI continue to increase, reaching a maximum at a ratio of 4 : 10, with the Pb(II) concentration in the solution reduced to trace levels. The removal efficiency of Pb(II) increased from 61.64% to approximately 100%, and the adsorption capacity increased from around 18.50 mg g^{-1} to 30 mg g^{-1}. The reason is that higher moisture content dissolves more Pb(II), and the addition of deionized water can partially remove water-soluble Pb(II). Fig. 5(b) shows that the addition of nZVI has distinct advantages, as it can react with both soluble and insoluble lead in the soil. On the other hand, deionized water mainly removes a portion of the soluble lead in the soil, and its removal efficiency shows an increasing trend followed by a decrease.[28] Water is a polar molecule that can provide H protons with strong reducibility for proton transfer and pollutant migration. The soil moisture content also affects the ionization and activation of zero-valent iron materials. Perhaps due to increasing soil moisture content, the concentration of dissolved oxygen in the solution can be reduced, thereby slowing down the oxidation rate of nano zero valent iron and improving remediation efficiency.[29]

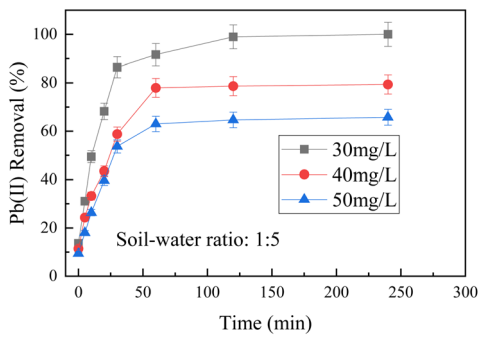

Fig. 4 Effect of initial concentration on the removal rate of Pb(II)using BC-nZVI.

3.4 The effect of initial pH value on the adsorption efficiency of Pb^{2+}

The pH value of the solution significantly influences the form of Pb(II) presence. Under weak alkaline conditions, Pb(II) precipitates as $Pb(OH)_2$ and is easily removed. However, under acidic conditions, Pb(II) primarily exists as Pb^{2+}. Therefore, this experiment investigated the removal efficiency of Pb(II) by BC-nZVI under pH conditions ranging from 1 to 6. Other experimental conditions included a temperature of 20 °C, initial Pb(II) concentration of 30 mg L^{-1}, BC-nZVI dosage of 1 g L^{-1}, and soil-to-water ratios of 1 : 5 and 3 : 10. The experimental results in Fig. 6(c) illustrate a gradual increase in the maximum removal by pH at different initial soil–water volume ratios. Upon comparison, it was determined that the difference in removal was negligible at varying soil/water volume ratios. This phenomenon can be attributed to two processes. Firstly, the extraction of Pb(II) by water is dependent on the volume ratio of soil to water. As the volume ratio of soil to water increases, the initial Pb ion concentration is lower in a soil/water ratio of 3 : 10 (approximately 25.30 mg L^{-1}) compared to a soil/water ratio of 1 : 5 (approximately 26.0 mg L^{-1}) at a pH of 6. This may account for the higher removal rate in the former than the latter. Additionally, the higher water solubility leads to increased dissolution of Pb(II), resulting in a higher maximum adsorption

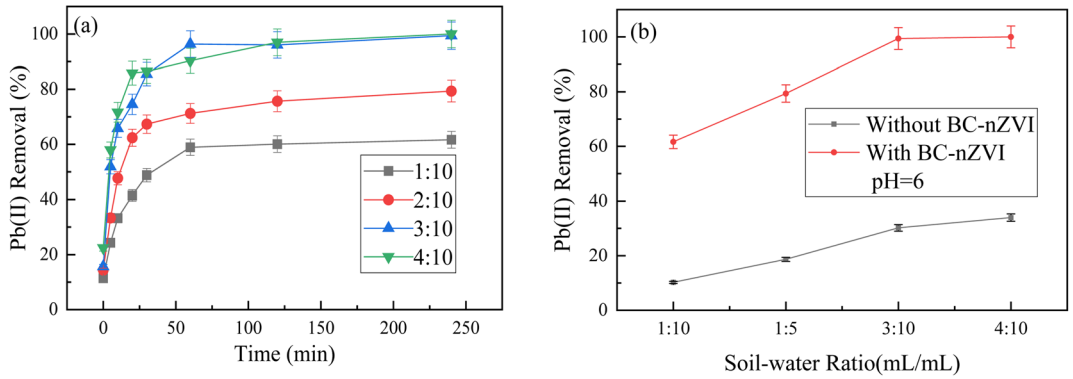

Fig. 5 Effect of initial concentration on the removal rate of Pb(II)using BC-nZVI.

rate of Pb ions. The addition of water can also aid in removing water-soluble Pb(II), thereby enhancing the adsorption of Pb(II) on the composites' surface.

The experimental results suggest that BC-nZVI exhibits rapid adsorption rates over a wide range of pH values, particularly at lower initial concentrations. For instance, at an initial pH of 6 and a soil-to-water ratio of 1 : 5, the Pb(II) removal rate reaches 99.36% within 120 minutes. However, as the pH gradually decreases to 1, the removal rate ultimately decreases to 48.63%. With a soil-to-water ratio of 3 : 10, the removal rate decreases from 99.41% to 53.41%. Under lower pH values, the increased concentration of H^+ enhances the competition between H^+ and Pb(II) cations for vacant adsorption sites. Additionally, when the pH is below the isoelectric point of BC-nZVI, the active sites on the surface of nZVI particles carry more positive charges, which repel metal cations. Pb(II) precipitates at pH values above 5.5. Therefore, as the pH increases, Pb(II) is more likely to form $Pb(OH)_2$ precipitates on the surface of BC-nZVI and be captured. Consequently, in acidic environments, increasing the pH of the solution as much as possible has a positive impact on the adsorption process. No transient enhancement in adsorption capacity is observed during the pH decrease. Instead, BC-nZVI exhibits a clear trend of increased removal of Pb(II) with increasing pH value.

3.5 The effect of initial temperature on the adsorption efficiency of Pb^{2+}

The impact of temperature on the adsorption of Pb(II) by BC-nZVI was examined under specific conditions: pH 6, soil-to-water ratio of 1 : 5, and BC-nZVI dosage of 1 g L^{-1}. The

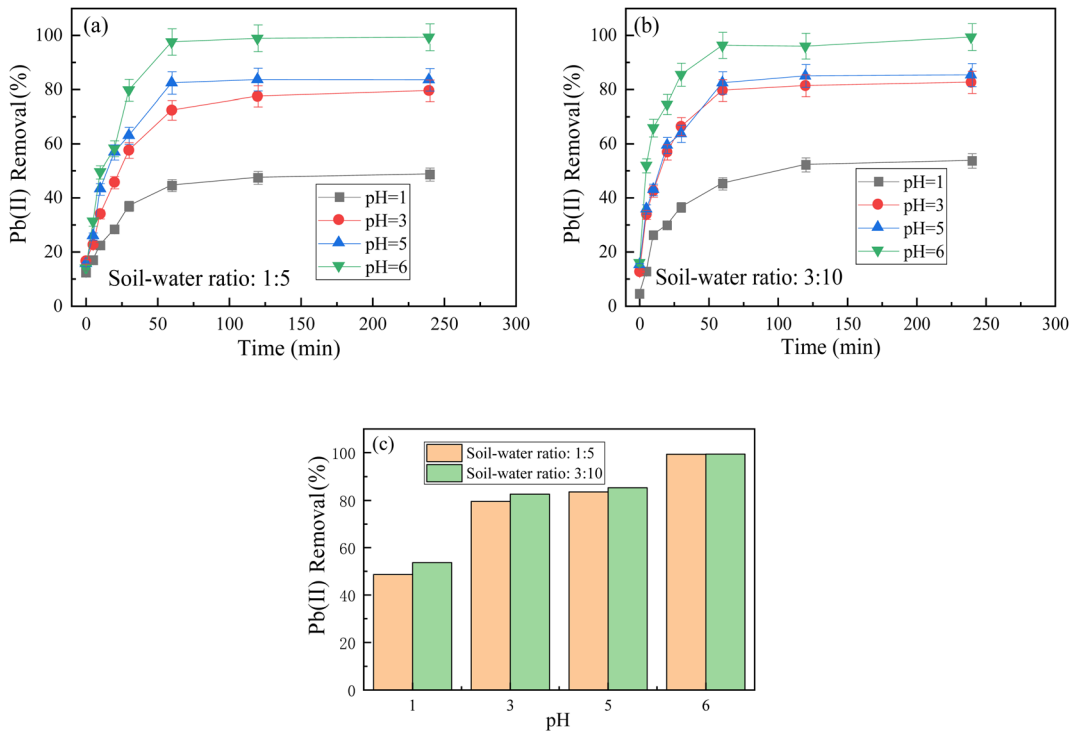

Fig. 6 The effect of different pH values on soil-to-water ratios of 1 : 5 and 3 : 10. (a and b), and the maximum removal rate of different initial soil moisture content at the same pH (c).

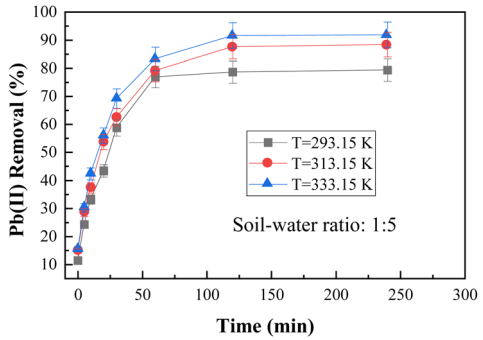

Fig. 7 Effect of temperature on the removal rate of Pb(II) using BC-nZVI.

experiment was carried out at various environmental temperatures (293.15 K, 313.15 K, and 333.15 K) throughout the adsorption process. Fig. 7 illustrates the different characteristics of the adsorption process at different temperatures. Fig. 7 illustrates that the removal efficiency of Pb(II) by BC-nZVI rises with increasing temperature. As the temperature rose from 293.15 K to 333.15 K, the efficiency of Pb(II) removal saw a significant improvement, jumping from 79.36% to 91.87% within a 120 minute timeframe. This uptick in temperature proved advantageous for the extraction of Pb(II), as it led to a greater number of activated molecules and facilitated the migration of Pb(II) from the solution to the adsorbent surface. Consequently, the adsorption process accelerated, and the BC-nZVI surface active sites became more accessible, ultimately resulting in the observed increase in removal rate.[30]

3.6 Reaction kinetics

3.6.1 Quasi first and second order dynamic models. The experiment was conducted with different initial concentrations of Pb(II) (30, 40, and 50 mg L^{-1}). The removal process at various time intervals (5, 10, 20, 30, 60, 120, and 240 minutes) was simulated using the linear fitting of the pseudo-first-order kinetic model ($R_1^2 = 0.94259$) and the pseudo-second-order kinetic model. Fig. 8 illustrates the linear fitting results of the pseudo-first-order and pseudo-second-order kinetic models for the Pb(II) removal process.

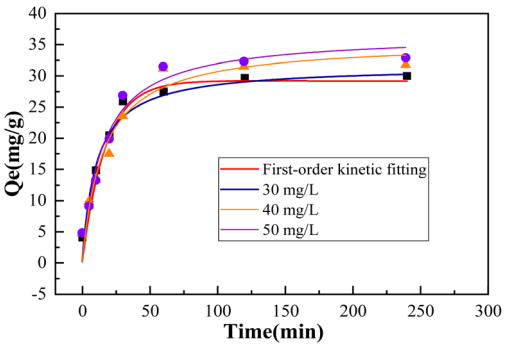

Fig. 8 Quasi first and second order kinetic linear fitting results of Pb(II) removal process.

From the data depicted in Fig. 8, it's evident that both the pseudo-first-order and pseudo-second-order kinetic models align well with the experimental data across various initial concentration conditions. As time progresses, the removal of Pb(II) steadily improves, with the pseudo-second-order kinetic model ($R_2^2 = 0.96229$) offering a more precise depiction of the removal process. Additionally, higher initial concentrations lead to faster removal rates and shorter time required to reach equilibrium, indicating that the rate-controlling step in the adsorption process may be a crucial factor.[31] The excellent agreement of the experimental results with the pseudo-second-order kinetic model indicates that the adsorption of heavy metal ions by BC-nZVI is predominantly a chemical adsorption process.[32] In chemical adsorption, the adsorption capacity directly correlates with the number of active sites on the adsorbent's surface. As a result, the removal kinetics vary with changes in the initial pollutant concentration. The kinetic parameters acquired *via* linear regression analysis are outlined in Table 1. It's noticeable from the table that elevated initial concentrations lead to increased final adsorption capacity (q_e).

3.6.2 Internal diffusion model. To comprehend the diffusion mechanisms involved in the adsorption process, including external mass transfer (boundary layer diffusion) and internal surface diffusion, we employed a particle internal diffusion model to analyze the kinetic data. If internal diffusion exclusively governs the rate-controlling step, the fitting line will pass through the origin. Otherwise, boundary layer diffusion to some extent controls the adsorption process.[33,34]

Fig. 9 illustrates the results of the linear fitting of the internal diffusion model for the Pb(II) removal process at a soil–water volume ratio of 1°:°5. The figure illustrates that the adsorption process of Pb(II) is nonlinear across the entire duration, implying the influence of multiple processes on adsorption. None of the experiments reveal a diffusion stage, suggesting that under the experimental conditions, the adsorption of Pb(II) on BC-nZVI may solely involve surface adsorption. The diffusion mechanism illustrated in Fig. 9 comprises three stages, aiding in the interpretation of the flake-like structure observed in TEM images of BC-nZVI. The initial stage (I) is linked to surface diffusion resulting from external surface complexation and instantaneous electron transfer, whereas the subsequent stage (II) entails a gradual transfer from the boundary to the core of BC-nZVI as the metal ion concentration diminishes. The concluding stage (III) represents a gradual equilibrium process, possibly driven by increased repulsion between cations.[35–37] Nevertheless, the entire Pb(II) curve exhibits non-linearity, suggesting that the internal diffusion model serves as a secondary rate-limiting step. It implies the presence of other mechanisms,

Table 1 Kinetic parameters obtained by linear regression analysis

Heavy metal ion	Initial concentration/(mg L^{-1})	q_e/(mg g^{-1})	R^2
Pb	30	Around 30.00	0.96229
	40	Around 31.774	0.94126
	50	Around 32.87	0.94916

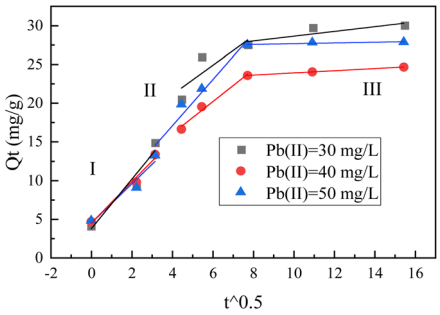

Fig. 9 Linear fitting results of internal diffusion model for and Pb(II) removal process.

such as surface mass transfer, which may contribute to the overall process.

3.7 Reaction thermodynamics

Thermodynamic parameters are important factors that determine the feasibility of adsorption processes. In this study, entropy change (ΔS^0), enthalpy change (ΔH^0), and standard free energy change (ΔG^0) were used to investigate the energy and spontaneity involved in the binding of Pb(II) with BC-nZVI at a soil–water volume ratio of 1°:°5. The lnkC *versus* 1/T Van't Hoff plot was constructed, as shown in Fig. 10. The Van't Hoff plots for all heavy metal elements exhibits a linear relationship. Therefore, the slope and intercept of the linear fitting results can be used to determine ΔH^0 and ΔS^0. The fitting correlation results and the calculated values of ΔG^0 are presented in Table 2. From Table 2 and it can be observed that the calculated ΔG^0 values are negative, confirming the feasibility of the removal process and indicating spontaneous adsorption. This suggests that the degree of spontaneity of the reaction increases with increasing temperature, and it is feasible to enhance the removal efficiency by raising the temperature from a thermodynamic perspective.

The positive fitting result of ΔH^0 can be attributed to the exothermic nature of the chemical adsorption of BC-nZVI towards Pb(II), which is consistent with the observed phenomenon in the experiments.[38,39] In other words, as the temperature of the adsorption environment increases, the removal efficiency is enhanced.

The positive value of ΔS^0 indicates that a structural change has occurred between the adsorbate and the adsorbent, leading

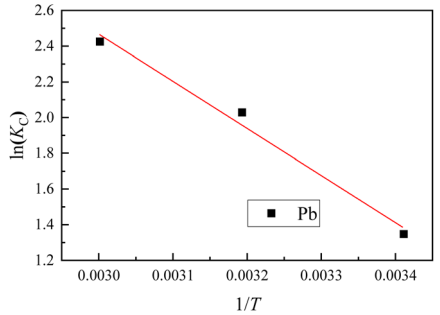

Fig. 10 Van't Hoff plots of the adsorption results of BC-nZVI on Pb(II).

Table 2 Thermodynamic fitting results of Pb(II) adsorption by BC-nZVI

Heavy metal ions	T/K	ΔS^0/(J mol^{-1} K)	ΔH^0/(kJ mol^{-1})	ΔG^0/(kJ mol^{-1})
Pb(II)	293.15			−3.282
	313.15	86.448	21.977	−5.282
	333.15			−6.716

to an increase in disorder. This suggests a potential chemical transformation between the heavy metal ions and BC-nZVI, emphasizing the material's affinity for Pb(II).[40] The positive value of ΔS^0 usually arises from the dehydration of metal ions and the breaking of hydration shells, partially explaining the positive value of ΔH^0, suggesting that the dehydration of Pb(II) and metal ions involves heat absorption.[41]

Additionally, the data also show that $|\Delta H^0| < |T\Delta S^0|$, suggesting that the adsorption process is primarily controlled by entropy rather than enthalpy.

3.8 Adsorption isotherms

The adsorption process is typically analyzed using Langmuir and Freundlich isotherms to depict the interaction between the adsorbent and adsorbate. In this study, equilibrium data from kinetic investigations were utilized to generate the adsorption isotherm of Pb(II) against the corresponding equilibrium concentration at 20 °C, yielding the adsorption isotherm curve. The Langmuir and Freundlich models were then applied to these data, as shown in Fig. 11. From the graph, it can be observed that the Langmuir model provides a better fit. The Langmuir model was used to determine the maximum adsorption capacity (q_{max}) of different BC-nZVI for various heavy metal ions, with Pb(II) being 32.87 mg g^{-1}. The experimental data exhibits a higher R^2 value for the Langmuir model compared to the Freundlich model, indicating that the interaction between BC-nZVI and Pb(II) is a result of chemical adsorption ($R_{Langmuir}^2 = 0.98407 > R_{Freundlich}^2 = 0.96436$). Furthermore, the adsorption process conforms more closely to the Langmuir model's assumption of monolayer and uniform adsorption.[42] In essence, this indicates a uniform distribution of binding energy across the adsorbent surface and no interaction among the adsorbates. The Pb(II) forms a fixed monolayer coverage on the surface of BC-nZVI.

3.9 Mechanism of lead removal by nano zero valent iron

Based on previous experimental results, a reasonable mechanism for removing Pb(II) has been proposed, as shown in Fig. 12. This mechanism involves the following steps: initially, Pb(II) is adsorbed onto the surface of biochar and nZVI *via* electrostatic interactions, subsequently undergoing reduction to Pb(0). Biochar potentially offers additional surface active sites through its oxygen functional groups, thus synergistically adsorbing Pb(II).[43] Additionally, Pb(II) interacts with the hydroxyl functional groups (Fe–OH) present on the surface of BC-nZVI, leading to removal *via* precipitation/co-precipitation processes. In conclusion, the mechanism for Pb(II) removal

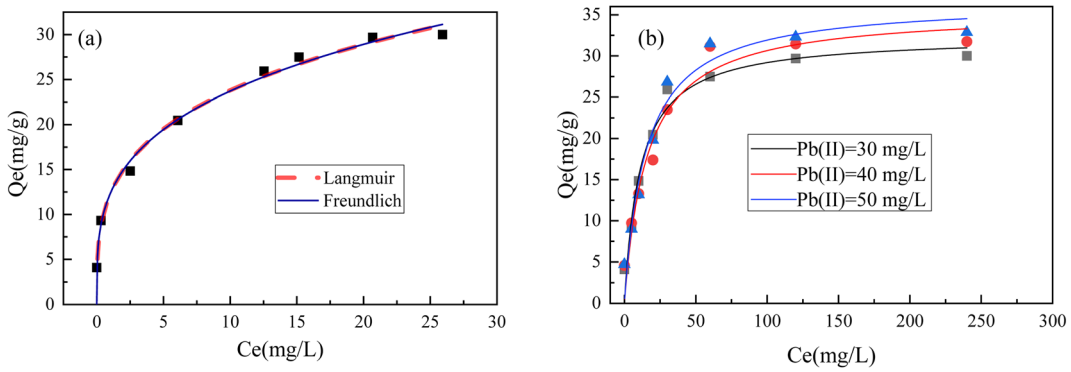

Fig. 11 Fitting results of Langmuir model (a) and Freundlich model (b) of Pb(II).

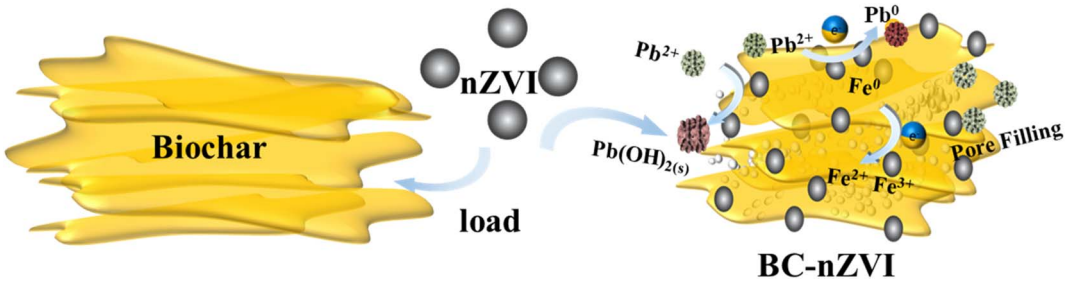

Fig. 12 Proposed a mechanism diagram for the adsorption and reduction of Pb(II) by BC-nZVI.

can be described by eqn (3) and (4), wherein BC-nZVI augments Pb(II) adsorption *via* a combined effect of electrostatic attraction, complexation, chemical precipitation, and reduction.

$$Pb^{2+} + Fe - OH \rightarrow Fe - O - Pb^{+} + H^{+} \text{ (adsorption)} \quad (3)$$

$$Pb^{2+} + -OH \rightarrow Pb^{2+} - OH \text{ (complexation)} \quad (4)$$

3.10 Magnetic separation of BC-nZVI

Fig. 13 illustrates the dispersion effect of shaking BC-nZVI and Pb(II) mixture, as well as the magnetic separation effect of BC-nZVI under an external magnetic field. Research findings indicate that BC-nZVI exhibits excellent dispersion in Pb(II) solution, possibly due to its magnetic properties. After adsorbing Pb(II), BC-nZVI uniformly attaches to the soil surface. To achieve efficient recovery, the reacted soil is vacuum-dried (60 °C, 4 hours) and then subjected to magnetic recovery using a plastic bag and tissue-wrapped magnet. As depicted in Fig. 13(a) and (b), the soil treated with BC-nZVI exhibits favorable magnetic properties, facilitating its easy recovery.Additionally, the external magnetic field can significantly accelerate the separation of BC-nZVI and pollutants, further verifying the feasibility of efficient recovery of BC-nZVI through magnetic separation technology.[44,45] In conclusion, BC-nZVI, as an

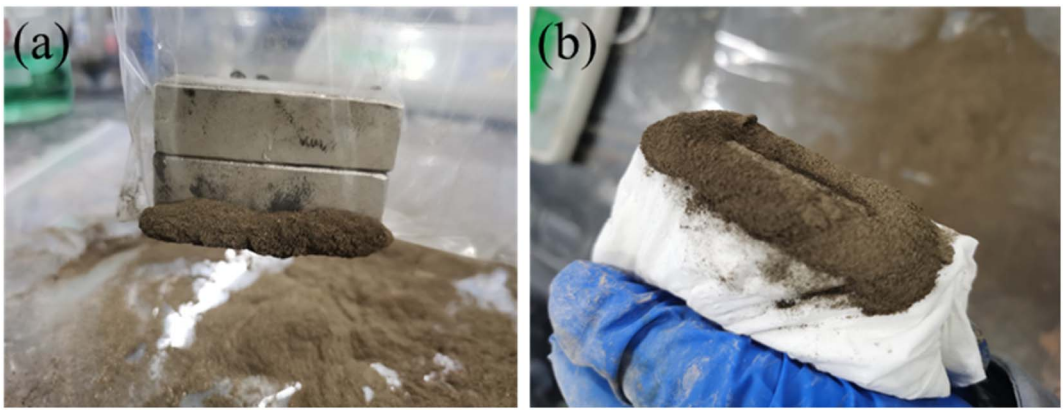

Fig. 13 Dispersion (a) and magnetic separation (a) and (b) effect of BC-nZVI in Pb(II)solution.

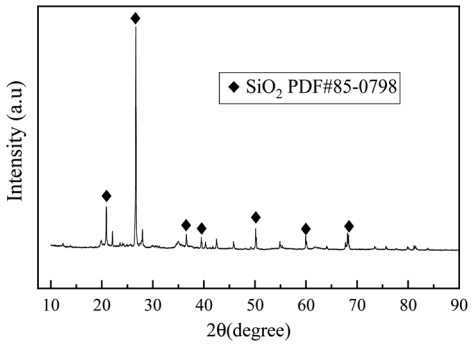

Fig. 14 XRD results of the reaction of BC-nZVI with Pb(II).

effective pollutant removal agent, has the potential to be efficiently recovered through magnetic separation technology in practical applications.

The recovered soil after reaction was subjected to vacuum drying, grinding treatment, and XRD detection. Fig. 14 shows The result of XRD is the soil sample after the reaction of BC-nZVI with Pb(II), The peaks at 26.75°, 20.89°, and 50.28° represent SiO_2. Pb(II) interacts with the hydroxyl functional groups (Fe–OH) on the surface of Fe_3O_4 and is removed through precipitation/co precipitation. However, no characteristic peaks related to Fe and Pb(II) are observed, which may be due to insufficient Fe and Pb content or poor crystallinity of the adsorbed products.

4 Conclusion

This study explored a cost-effective and straightforward method for synthesizing magnetic sheet-like BC-nZVI materials through rheological phase reaction, which effectively solved the heavy metal pollution problem in wastewater and avoided using expensive reducing agents. The physical and chemical properties as well as the fine structure of the materials were characterized by multiple methods. Meanwhile, various influencing factors on the removal efficiency of lead were investigated, and the removal process was analyzed by multiple classic models. The following conclusions can be drawn.

(1) The BC nZVI composite material prepared by rheological phase reaction uniformly disperses nZVI particles on the surface of BC, and the loading of biochar effectively reduces the aggregation degree of nZVI. The nZVI particles have a clear sheet-like structure, with a diameter between 50-1500 nm and a thickness less than 50 nm.

(2) Under the conditions of pH of 6, temperature of 20 °C, soil water ratio of 1 : 5, and BC-nZVI dosage of 1 g L^{-1}, it takes about 120 minutes for BC-nZVI to reduce Pb(II) content to trace levels when treating wastewater with an initial concentration of 30 mg L^{-1}. Raising the initial concentration diminishes Pb(II) removal efficiency but enhances adsorption capacity. With increasing soil–water volume ratio, the removal rate consistently rises. The optimal ratio is 4 : 10, achieving a removal rate of approximately 100%.

(3) The removal process of BC-nZVI follows a quasi-second-order kinetic model, while the adsorption isotherm aligns better with the Langmuir model, indicating a chemical adsorption process. According to the Langmuir model, the adsorption capacity of Pb(II) is 32.87 mg g^{-1}. Thermodynamic analyses indicate that the removal process is spontaneous. The enrichment of Pb(II) by BC-nZVI primarily involves adsorption co-precipitation.

Overall, this study offers valuable references for selecting nZVI carrier materials, advancing environmental remediation techniques, and particularly for heavy metal removal.

Author contributions

Shuxian Wei: conceptualization, methodology, software, investigation, formal analysis, writing – original draft visualization; Gang Du: data curation, writing – original draft; Canhua Li (corresponding author): investigation; conceptualization, funding acquisition, resources, supervision; Lanyue Zhang: resources, supervision; Jiamao Li: software, validation, writing – review & editing; Aiqin Mao: visualization, writing – review & editing; Chuan He: funding acquisition, resources, supervision.

Conflicts of interest

The authors declare that they have no known competing financial interests or personal relationships that could have appeared to influence the work reported in this paper.

Acknowledgements

We are grateful to the sponsors of this work. Anhui University of Technology, School of Metallurgical Engineering and School of Materials Science and Engineering, Guangxi Academy of Sciences, Research Center for Low Carbon Utilization of Bulk Solid Waste, Anhui Provincial Central Leading Local Science and Technology Development Special Project (No. 202107d06050012); Anhui University Graduate Scientific Research Project (No. YJS202110333); Gansu Province University Teacher Innovation Fund Project, (No. 2024B-342).

References

1 K. Lei, E. Giubilato, A. Critto, *et al.*, Contamination and human health risk of lead in soils around lead/zinc smelting areas in China, *Environ. Sci. Pollut. Res.*, 2016, **23**(13), 13128–13136, DOI: **10.1007/s11356-016-6473-z**.

2 J. J. Li, H. Ma, H. Yu, *et al.*, Effect and potential mechanisms of sludge-derived chromium, nickel, and lead on soil nitrification: Implications for sustainable land utilization of digested sludge, *J. Hazard. Mater.*, 2024, **133552**(466), 0304–3894, DOI: **10.1016/2024.133552**.

3 J. F. Zhu, W. C. Gao, W. T. Zhao, *et al.*, Wood vinegar enhances humic acid-based remediation material to solidify Pb(II) for metal-contaminated soil, *Environ. Sci. Pollut. Res.*, 2021, **28**(10), 12648–12658, DOI: **10.1007/s11356-020-11202-3**.

4 S. Dubey, S. Banerjee, S. N. Upadhyay, *et al.*, Application of common nano-materials for removal of selected metallic

species from water and wastewaters: A critical review, *J. Mol. Liq.*, 2017, **240**, 656–677, DOI: 10.1016/j.molliq.2017.05.107.

5 Y. L. Hua, D. H. Li, T. H. Gu, *et al.*, Enrichment of uranium from aqueous solutions with nanoscale zero-valent iron: surface chemistry and application prospect, *Acta Chim. Sin.*, 2021, **79**(8), 1008–1022, DOI: 10.6023/A21040160.

6 H. B. Liu, J. Wen, Q. T. Liu, *et al.*, Enhanced performances of anaerobic digestion processes treating organic wastes: Role of iron and carbon based nanomaterials, *Surf. Interfaces*, 2023, (43), 103548, DOI: 10.1016/j.surfin.2023.103548.

7 T. Bandara, A. Franks, J. M. Xu, *et al.*, Chemical and biological immobilization mechanisms of potentially toxic elements in biochar-amended soils, *Crit. Rev. Environ. Sci. Technol.*, 2020, **50**(9), 903–978, DOI: 10.1080/10643389.2019.1642832.

8 D. Peng, B. Wu, H. Tan, *et al.*, Effect of multiple iron-based nanoparticles on availability of lead and iron and micro-ecology in lead contaminated soil, *Chemosphere*, 2019, **228**, 44–53, DOI: 10.1016/2019.04.1060045-6535.

9 Y. Lu, X. Y. Jin, Q. Lin, *et al.*, Enhanced adsorption and reduction of Pb(II) and Zn(II) from mining wastewater by carbon@nano-zero-valent iron (C@nZVI) derived from biosynthesis, *Sep. Purif. Technol.*, 2023, **123249**(31), 1383–5866, DOI: 10.1016/j.seppur.2023.123249.

10 W. Qian, J. Y. Liang, W. X. Zhang, *et al.*, A porous biochar supported nanoscale zero-valent iron material highly efficient for the simultaneous remediation of cadmium and lead contaminated soil, *J. Environ. Sci.*, 2022, **113**, 231–241, DOI: 10.1039/c6ra27256h.

11 Z. Chen, J. Shen, X. Xu, *et al.*, Adsorption of antibiotic, heavy metal and antibiotic plasmid by a wet-state silicon-rich biochar/ferrihydrite composite to inhibit antibiotic resistance gene proliferation/transformation, *Chemosphere*, 2023, **324**, 138356, DOI: 10.1016/j.chemosphere.2023.138356.

12 C. M. Wang, D. Bare, J. Amonette, *et al.*, Morphology and electronic structure of the oxide shell on the surface of iron nanoparticles, *J. Am. Chem. Soc.*, 2009, **131**(25), 8824–8832, DOI: 10.1021/ja900353f.

13 C. Lei, J. k. Zhang, Q. G. Li, *et al.*, Removal of p-nitrophenols by BC@nZVI activated persulfate: A study of key factors and mechanisms, *J. Environ. Chem. Eng.*, 2023, **111483**(6), 2213–3437.

14 S. W. Zhang, L. X. Zhang, S. L, *et al.*, Study on the fluorescence properties of carbon dots prepared *via* combustion process, *Lumines*, 2019, (206), 608–612, DOI: 10.1016/j.jlumin.2018.10.086.

15 Z. Chen, J. Shen, X. Xu, *et al.*, Adsorption of antibiotic, heavy metal and antibiotic plasmid by a wet-state silicon-rich biochar/ferrihydrite composite to inhibit antibiotic resistance gene proliferation/transformation, *Chemosphere*, 2023, **324**, 138356–138370, DOI: 10.1016/j.chemosphere.2023.138356.

16 C. He, Y. R. Ding, C. H. Li, *et al.*, Cost-effective core@shell structured zero-valent iron nanoparticles @ magnetic (nZVI@Fe_3O_4) for Cr(VI) removal from aqueous solutions: preparation by disproportionation of Fe(II), *RSC Adv.*, 2023, **13**, 26983, DOI: 10.1039/d3ra03133k.

17 X. Yang, A. D. Igalavithana, S. E. Oh, *et al.*, Characterization of bioenergy biochar and its utilization for metal/metalloid immobilization in contaminated soil, *Sci. Total Environ.*, 2018, (640), 704–713, DOI: 10.1016/j.scitotenv.2018.05.298.

18 R. P. Lopes and D. Astruc, Biochar as a support for nanocatalysts and other reagents: Recent advances and applications, *Coord. Chem. Rev.*, 2021, **426**, 213585, DOI: 10.1016/j.ccr.2020.213585.

19 E. M. Carrera, K. S. Lin, M. T. Weng, *et al.*, In vitro studies of Pluronic F127 coated magnetic silica nanocarriers for drug delivery system targeting liver cancer, *Eur. Polym. J.*, 2021, **153**, 110504, DOI: 10.1016/j.eurpolymj.2021.110504.

20 J. Hu, G. H. Chen and Lo Irenemc, Removal and recovery of Cr(VI) from wastewater by maghemite nanoparticles, *Water Res.*, 2005, **39**(18), 4528–4536, DOI: 10.1016/j.watres.2005.05.051.

21 S. F. Lim, Y. M. Zheng and J. P. Chen, Organic arsenic adsorption onto a magnetic sorbent, *Langmuir*, 2009, **25**(9), 4973, DOI: 10.1021/la802974x.

22 E. A. Deliyanni, L. Nalbandian and K. A. Matis, Adsorptive removal of arsenites by a nanocrystal lline hybrid surfactant-akaganeite sorbent, *J. Colloid Interface Sci.*, 2006, **302**(2), 66–458, DOI: 10.1016/j.jcis.2006.07.007.

23 S. Z. Guo, K. L. WU, Y. Gao, *et al.*, Efficient removal of Zn(II), Pb(II), and Cd(II) in waste water based on magnetic graphitic carbon nitride materials with enhanced adsorption capacity, *J. Chem. Eng. Data*, 2018, **63**(10), 3902–3912, DOI: 10.1039/c5ta08106h.

24 C. L. Jiao, *Application of Carbon Modified Nano-Zero-Valent-Iron in Treartment of Chromium Pollution [D]*, Beijing University of Chemical Technology, Beijing, 2018.

25 J. Liu, G. Xiao, X. Ye, *et al.*, 3D graphene/δ-MnO2 aerogels for highly efficient and reversible removal of heavy metal ions, *J. Mater. Chem.*, 2016, **4**(5), 1970–1979, DOI: 10.1039/c5ta08106h.

26 L. Signorini, L. Pasquini, L. Savini, *et al.*, Size-dependent oxidation in iron oxide core-shell nanoparticles, *Phys. Rev. B*, 2003, **68**, 195423, DOI: 10.1103/PhysRevB.68.195423.

27 X. D. Zhang, D. Y. Shi, X. Li, *et al.*, Nanoscale dispersing of zero-valent iron on $CaCO_3$ and their significant synergistic effect in high performance removal of lead, *Chemosphere*, 2019, **224**, 390–397, DOI: 10.1016/j.chemosphere.

28 X. L. Xu, *Study on the Preparation of Stabilized Nanometer Zero-Valent Iron and Application of Hexavalent Chromium Pollution in Environmental treatment[D]*, Qingdao University of Science and Technology, Shandong, 2017.

29 Y. Ying, W. Xie, *et al.*, Remediation and phytotoxicity of decabromodiphenyl ether contaminated soil by zero valent iron nanoparticles immobilized in mesoporous silica microspheres, *J. Environ. Manage.*, 2016, **166**, 478–483, DOI: 10.1016/j.jenvman.2015.10.042.

30 M. Arshadi, M. Soleymanzadeh, J. Salvacion, *et al.*, Nanoscale zero-valent iron (nZVI) supported on sineguelas waste for Pb(II) removal from aqueous solution: kinetics,

thermodynamic and mechanism, *J. Colloid Interface Sci.*, 2014, **426**, 241–251.

31 X. S. Lv, X. Q. Xue, G. M. Jiang, *et al.*, Nanoscale zero-valent iron (nZVI) assembled on magnetic Fe_3O_4/graphene for chromium (VI) removal from aqueous solution, *J. Colloid Interface Sci.*, 2014, **417**, 51–59, DOI: **10.1016/j.jcis.2013.11.044**.

32 M. Arshadi, M. K. Abdolmaleki, F. Mousavinia, *et al.*, Nano modification of nZVI with an aquatic plant Azolla filiculoides to remove Pb(II) and Hg(II) from water: aging time and mechanism study, *J. Colloid Interface Sci.*, 2017, **486**, 296–308, DOI: **10.1016/j.jcis.2016.10.002**.

33 M. Nikazar, M. Alizadeh, R. Lalavi, *et al.*, The optimum conditions for synthesis of Fe_3O_4/ZnO core/shell magnetic nanoparticles for photodegradation of phenol, *J. Environ. Health Sci. Eng.*, 2014, **12**(1), 21, DOI: **10.1186/2052-336X-12-21**.

34 L. Yang, X. Y. Jin, Q. Lin, *et al.*, Enhanced adsorption and reduction of Pb(II) and Zn(II) from mining wastewater by carbon@nano-zero-valent iron (C@nZVI) derived from biosynthesis, *Sep. Purif. Technol.*, 2023, **123249**, 714–720, DOI: **10.1016/j.seppur.2023.123249**.

35 Y. Qu, L. C. Liu, *et al.*, Green synthesis of hydrophilic activated carbon supported sulfide nZVI for enhanced Pb(II) scavenging from water: Characterization, kinetics, isotherms and mechanisms, *J. Hazard. Mater.*, 2021, (403), 123607, DOI: **10.1016/j.jhazmat.2020.123607**.

36 J. Yan and K. Li, A magnetically recyclable polyampholyte hydrogel adsorbent functionalized with β-cyclodextrin and graphene oxide for cationic/anionic dyes and heavy metal ion wastewater remediation, *Sep. Purif. Technol.*, 2021, (277), 119469, DOI: **10.1016/j.seppur.2021.119469**.

37 T. C. Nguyen, P. Loganathan, T. V. Nguyen, *et al.*, Naidu Simultaneous adsorption of Cd, Cr, Cu, Pb, and Zn by an iron-coated Australian zeolite in batch and fixed-bed column studies, *Chem. Eng.*, 2015, (270), 393–404, DOI: **10.1016/j.cej.2015.02.047**.

38 J. Liu, L. Huang, G. Peng, *et al.*, Removal of Cr(VI) from water by granular activated carbon supported nanoscale zero-valent iron, *Chin. J. Process Eng.*, 2019, **19**(4), 714–720, DOI: **10.12034/j.issn.1009-606X.218294**.

39 H. B. Zhang, Z. F. Tong, T. Y. Wei, *et al.*, Removal characteristics of Zn(II) from aqueous solution by alkaline Ca-bentonite, *Desalination*, 2011, **276**(1–3), 103–108, DOI: **10.1016/j.desal.2011.03.026**.

40 S. M. Yang, A. R. Liu, J. Liu, *et al.*, Advance of sulfidated nanoscale zero-valent iron: synthesis, properties and environmental application, *Acta Chim. Sin.*, 2022, **80**(11), 1536–1554, DOI: **10.6023/A22080345**.

41 M. Z. Chen, H. Xu, Y. J. Zhang, *et al.*, Effective removal of heavy metal ions by attapulgite supported sulfidized nanoscale zerovalent iron from aqueous solution, *Colloids Surf., A*, 2022, **640**, 128192, DOI: **10.1016/j.colsurfa.2021.128192**.

42 L. Yang, X. Y. Jin, Q. Lin, *et al.*, Enhanced adsorption and reduction of Pb(II) and Zn(II) from mining wastewater by carbon@nano-zero-valent iron (C@nZVI) derived from biosynthesis, *Sep. Purif. Technol.*, 2023, **311**, 123249, DOI: **10.1016/j.seppur.2023.123249**.

43 J. Dai, Z. Wang, K. Chen, *et al.*, Applying a novel advanced oxidation process of biochar activated periodate for the efficient degradation of bisphenol A: Two nonradical pathways, *Chem. Eng.*, 2023, **453**, 139889, DOI: **10.1016/j.cej.2022.139889**.

44 H. R. Xiang, X. B. Min, C. J. Tang, *et al.*, Recent advances in membrane filtration for heavy metal removal from wastewater: a mini review, *J. Water Proc.engineering*, 2022, **49**, 103023, DOI: **10.1016/j.jwpe.2022.103023**.

45 T. H. Gu, J. M. Shi, Y. L. Hua, *et al.*, Enrichment of silver from water using nanoscale zero-valent iron (nZVI), *Acta Chim. Sin.*, 2017, **75**(10), 991–997, DOI: **10.6023/A17070345**.